
Article:
Reynolds, Carl, Thompson, Richard and McLeish, Tom orcid.org/0000-0002-2025-0299 (2018) Pressure and shear rate dependence of the viscosity and stress relaxation of polymer melts. Journal of Rheology. pp. 631-642. ISSN 1520-8516

https://doi.org/10.1122/1.5012969

Pressure and shear rate dependence of the viscosity and stress relaxation of polymer melts

Carl Reynolds, Richard Thompson, and Tom McLeish

Citation: Journal of Rheology **62**, 631 (2018); doi: 10.1122/1.5012969
View online: https://doi.org/10.1122/1.5012969
View Table of Contents: http://sor.scitation.org/toc/jor/62/2
Published by the The Society of Rheology

Pressure and shear rate dependence of the viscosity and stress relaxation of polymer melts

Carl Reynolds,[a] Richard Thompson, and Tom McLeish

Department of Chemistry, Durham University, Lower Mountjoy, South Road, Durham DH1 3LE, United Kingdom

(Received 9 November 2017; final revision received 10 February 2018; published 2 March 2018)

Abstract

The pressure dependencies of polymer viscosity and stress relaxation are an important but often overlooked aspect of the material processing and postprocessing properties. We show how these dependencies can be isolated in a single measurement and can be related to the characteristic relaxation times of the material. Using a multipass rheometer (a small volume double piston rheometer), a polystyrene melt was confined at 170 °C and pressure range 1–100 bar. The pressure drop over a contraction-expansion geometry and stress birefringence were monitored as a function of shear rate, shear history, and applied pressure. Relaxation times, extracted from the stress decays correspond closely to the Rouse and reptation times of the polymer and the contributions of each mode are determined by the relationship between the shear rate and relaxation times established from linear rheology. Increasing the applied pressure caused an increase in viscosity and the measured relaxation time, but no effect on relaxation times was observed with shear rate. The technique allows the extraction of relaxation data following deformation at high shear rates and pressures, conditions more akin to industrial processing than conventional shear rheology. © *2018 The Society of Rheology*. https://doi.org/10.1122/1.5012969

I. INTRODUCTION

While time-temperature superposition principles [1] are routinely used throughout polymer rheology, the pressure dependence of rheological properties is still usually ignored, despite being well known (for example, the reduction in free volume and resulting increase in modulus with increasing pressure is frequently noted [2,3]). This is in part because it is more challenging to address with standard instruments. For many rheological tests, relaxation times are collected from measurements on open systems such as shear rheometers where it is not feasible to pressurize the sample. However, when these results are then applied to simulations of industrial processes at high pressures (e.g., extrusion, injection moulding), the errors could easily result in using suboptimal processing conditions. Since the pressure dependence of viscosity was first noted [4], various studies have explored the nature of this dependence in relation to features such as the glass transition temperature [5] and free volume [6]. Pressure dependence of viscosity has generally been found to be greatest for materials that are close to their glass transitions, where it may be expected that a small change in free volume has a large influence on polymer chain dynamics.

One common way of quantitatively expressing the relationship between viscosity and applied pressure is the pressure-viscosity coefficient, which at a given temperature, is defined using the Barus equation [4],

$$\beta_{T,p} = \frac{d\,ln(\eta)}{dp}. \tag{1}$$

These values have been recorded for a variety of materials under different conditions (e.g., polyethylene [7], polymethyl methacrylate (PMMA) [7], and polystyrene (PS) [7–10]). Most commonly capillary rheometers have been used, usually with an adaptation to regulate the exit pressure [11]. Slit rheometers have also been used for this purpose, for example, Volpe *et al.* [9] adapted an injection moulding apparatus to perform narrow slit experiments, and Kadijk and van der Brule [12] used transducers mounted on the slit wall to remove the entry and exit effects.

Sedlacek *et al.* [7] observed that polyethylenes with their regular structure have the least pressure dependence and that adding branching causes pressure to have a greater effect (e.g., $\beta = 10.36\,\mathrm{GPa}^{-1}$ for high density polyethylene (HDPE) at 170–210 °C but $18.33\,\mathrm{GPa}^{-1}$ for low density polyethylene (LDPE) at 150–190 °C). Polymers with bulky side groups show greater pressure dependencies (e.g., $43.45\,\mathrm{GPa}^{-1}$ for PS at 162–242 °C and $43.57\,\mathrm{GPa}^{-1}$ for PMMA at 230–250 °C). On this basis, it appears that free volume is more significant to the pressure dependence of viscosity rather than other factors such as proximity to a melting transition. A similar trend is well established for the temperature dependence of relaxation time, whereby increasing temperature increases free volume [7,13,14].

However, there remains substantial debate on the universality of the β parameter. The pressure-viscosity coefficient has separately been reported to be both dependent and independent on temperature, pressure, shear rate, and results depend on whether shear or extensional viscosity is examined. Other coefficients have been proposed that encompass these dependencies (e.g., on shear rate [15]), but pose extra challenges to verify

[a]Author to whom correspondence should be addressed; electronic mail: c.d.reynolds@durham.ac.uk

experimentally. Cardinaels *et al.* [15] have evaluated different methods for calculating the β parameter and concluded that in order to give a true thermodynamic property of the melt, β at constant shear stress was required. The shear rate independent β could still be used, but at high shear rates would include contributions from shear thinning, and hence could be more difficult to interpret. The β value is also seen to vary by measurement technique, which is likely due to the different type of flow generated by different rheometers, for example, a high pressure sliding plate rheometer, which keeps shear rate and pressure uniform [16] was seen to give different values to a capillary rheometer [17], which is less well controlled.

The applicability of a multipass rheometer (MPR) for studying rheology under pressure has previously been established [18,19]. The enclosed system enabled oscillatory rheology to isolate the elastic and viscous moduli, which is not possible with other process-mimicking techniques such as capillary rheometry [10,20] and injection moulders [9,21]. The MPR could also access higher strains than are possible with a rotational rheometer as it does not suffer from sample loss so readily. Although the effects of pressure on steady shear and oscillatory viscosities have been examined previously, early experiments did not have the capability to observe the sample optically and significantly, could not analyze the relaxation of stress.

As well as the change in viscosity, some simulations [22,23] and dielectric experiments [24] have shown a corresponding increase of the relaxation times of polymers with increasing pressure, and show that the pressure dependence cannot be ignored. This is an important consideration for high pressure processes such as injection moulding, because residual stress in polymers can lead to significant problems of ageing and mechanical weakness in products. In this paper, we use a multipass rheometer (MPR4) to provide direct characterization of viscosity and relaxation as a function of shear rate and shear history. Because the MPR4 can measure pressure difference as well as provide visualization of stress relaxation, this approach provides a unique opportunity to study this relaxation under pressure. The principle of the MPR in its current form (shown in Fig. 1) was first described by Mackley [25], and its use is reviewed in detail by Mackley and Hassel [26]. The salient features for this work are that the MPR allows the extraction of both simple linear shear data (usually found using a rotational rheometer) and steady shear flow curves (usually found using capillary devices) and obtains both as a function of pressure, as well as pressure-drop, which can be controlled separately in this case [19].

Here, we report the use of a slit geometry with quartz windows at two faces to study stress decay as controlled deformations at high pressures were applied. The resulting decays of both pressure and stress (by examining the decay of stress fringes) are examined as a function of applied pressure and imposed shear rate. Careful analysis of the decay rate enables this to be related to the fundamental relaxation processes of this linear polymer and provides the starting point for predicting pressure dependent relaxation in more complex polymers.

The aim of this work is to provide a detailed interpretation of flow and relaxation under sustained pressure. By combining

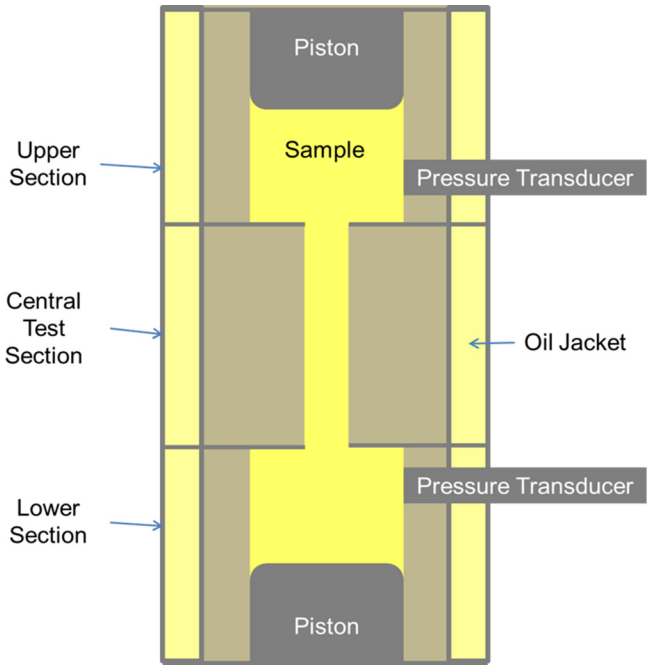

FIG. 1. Illustration of the multipass rheometer fitted with a narrow slit geometry.

MPR measurements with size exclusion chromatography (SEC) and rigorous linear rheology of test material, we probe the relationships between pressure, flow, viscosity, and relaxation times. This paper is set out as follows: Following the materials and experimental section, we report the linear shear rheology of a PS sample, which is analyzed in terms of the molecular weight distribution established by SEC. As well as providing the characteristic reptation and Rouse times of the full molecular weight distribution, this analysis allows these characteristic relaxation times to be calculated for different fractions of the distribution. Results for stress birefringence and pressure drop obtained with the multipass rheometer are outlined and analyzed to establish the reliability of the method to determine wall shear rates and relaxation times. Derived results for β as a function of flow rate obtained via pressure drop and optical analysis are compared, before we focus on the relaxation times. Stress relaxation cannot be characterized by a single relaxation time, but for most cases is well described by a superposition of two relaxation times; one which is close to the reptation time, and one which is close to the Rouse time, in accord with the standard minimal model emerging from tube theory of polymer melts in nonlinear response [27]. Finally, we show that the polydisperse nature of the polymer used here (and indeed for virtually all industrial polymers) has significant implications for stress relaxation.

II. EXPERIMENTAL

A. Materials

Polystyrene (PS) was supplied by Sigma Aldrich (SKU: 441147). The molecular weight distribution, $M_w = 315$ kg/mol, $M_n = 111$ kg/mol, was determined by Gel Permeation Chromatography using a Viscotek TDA 302 with triple

detection (Light scattering, viscosity, and refractive index) with tetrahydrofuran as solvent at 35 °C and a flow rate of 1 ml/min. The full distribution of molecular weight is given in supplementary material A [28].

B. Shear rheometry

To characterize the sample, a disk 1 mm thick with a diameter of 25 mm was pressed in a heated press at 150 °C under 5 tonnes pressure for 5 min. Rheological characterization of this material was performed on a TA AR-2000 rheometer equipped with 25 mm parallel plates and an environmental test chamber under nitrogen gas. Oscillatory frequency sweeps in the range 0.1–600 rad/s were performed at 1% strain, at temperatures between 130 and 210 °C. A Williams-Landel-Ferry (WLF) time-temperature superposition was applied using REPTATE software [29] to overlay the results to produce a single spectrum at a temperature of 170 °C.

C. Capillary rheometry

In order to extract steady shear viscosity of the sample, capillary rheometry was performed. Pellets of the sample were loaded into a twin bore Malvern RH2000 rheometer fitted with a capillary with diameter of 1.5, 1.0, or 0.5 mm each with a length/diameter ratio of 16 and a matching diameter orifice die. Measurements were performed at 170 °C at speeds of 0.1–10 mm/s. The Bagley correction [30] was applied for the exit and entry effects and the Rabinowitsch correction [3,31] made to the shear rates to account for shear thinning.

D. Multipass rheometry

The MPR4 was fitted with a contraction-expansion geometry, with dimensions as given in Fig. 2. Approximately 10 g of polystyrene pellets were loaded into the top and bottom reservoirs and heated to 170 °C with an oil bath connected to jackets around each of the sections, and monitored with three temperature sensors, one in each section. A light source was passed through a 514 nm filter, a linear polariser and a quarter wave plate. The resulting light was used to illuminate the sample through the quartz windows. Video of the sample was recorded during the measurement at 18 fps using a camera fitted with a circular polariser (a combined linear polariser and quarter wave plate) from the quartz window on the opposite side.

The single shot mode of the multipass rheometer was used in order to reach a steady state and then observe the resulting decay. The pistons were driven toward the geometry to give an initial pressure, before moving both together, one toward and one away from the test section, keeping the spacing constant, in order to create flow through the test section. Pressure transducers in the top and bottom reservoir walls were used to monitor the pressure drop across the geometry. Pressure was recorded at 200 Hz. After allowing sufficient time for a steady state in pressure drop to be reached and the stress fringes to become stable, the flow was stopped. The pressure and stress were continually monitored to observe the decay.

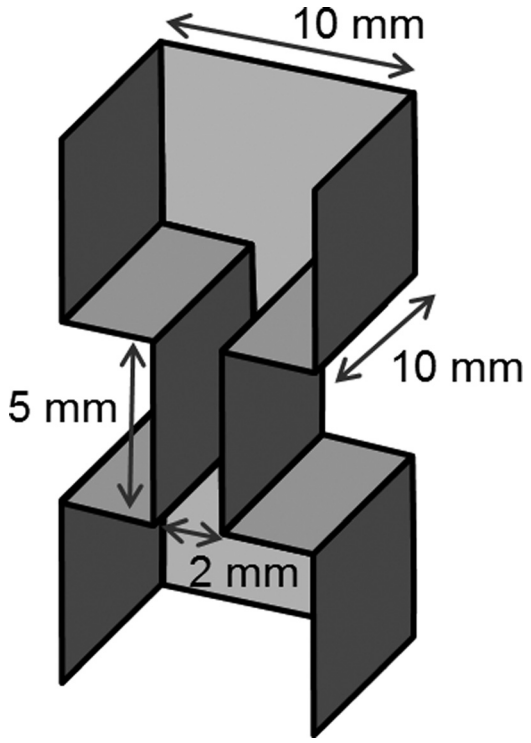

FIG. 2. Dimensions of the contraction-expansion geometry.

Wall shear rates were calculated using

$$\dot{\gamma} = \left(\frac{6Q}{w^2 d}\right)\left(\frac{2+n}{3}\right), \tag{2}$$

where w is the slit width (mm), d is the slit depth (mm), and Q is the fixed flow rate (mm^3/s), equal to the piston speed (mm/s) multiplied by the cross-sectional area of the reservoir [π*(*reservoir radius* (mm))^2]. n is the Rabinowitsch correction factor, determined as 1.59 from the gradient of a log(wall shear rate) vs log(stress) vs graph (plot is included in supplementary material A [28]).

Experiments were performed at piston speeds between 0.005 and 0.5 mm/s. The speeds were chosen to span from shear rates that are below both the inverse Rouse and reptation times, to those where both were exceeded (see Table I). For each piston speed, experiments were performed at initial pressures of 1, 3, 10, 30, and 100 bar. It is the initial pressure,

TABLE I. Piston speeds used in these experiments, and the corresponding flow rates in the reservoir, shear rate at the wall and the Rouse and reptation Weissenberg numbers, calculated using $\tau_D = 3.34$ s, the crossover point in the linear rheology, and $\tau_R = 0.434$ s taken from the fit to linear rheology.

Speed (mm s^{-1})	Flow rate (mm^3 s^{-1})	Apparent wall shear rate (s^{-1})	Rabinowitsch corrected shear rate (s^{-1})	Weissenberg number	
				Rouse	Reptation
0.005	0.39	0.059	0.071	0.031	0.24
0.01	0.79	0.12	0.14	0.061	0.47
0.05	3.9	0.59	0.71	0.31	2.4
0.1	7.9	1.2	1.4	0.61	4.7
0.5	39	5.9	7.1	3.1	24

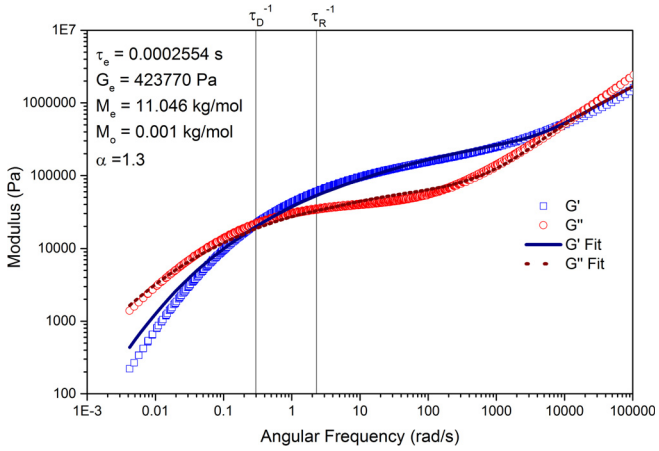

FIG. 3. Rheological spectrum of Aldrich polystyrene, a combination of measurements made between 130 and 210 °C and shifted to 170 °C using a WLF time temperature superposition with the parameters $C_1 = 5.15$, $C_2 = -60.3$, $Rho_0 = 0.950$ $C_3 = -5.14$. Also shown is a fit to the data using double reptation theory from the REPTATE [24] software package. Parameters used are labeled along with the Rouse time (extracted from the theory) and reptation time (crossover in G′ and G″). τ_e represents the Rouse time of one entanglement segment, G_e is the entanglement modulus, M_e is the entanglement molecular weight, M_0 is the molecular weight of a Rouse monomer, and α is the constraint release parameter.

applied to the sample before starting the pistons that is used to compare the results. From this point "pressure" will refer to the pressure initially applied to the sample, and "pressure drop" will refer to the difference between the values recorded by the two transducers.

III. RESULTS

A. Shear rheology

The shear rheology results are shown in Fig. 3. A fit was performed using double reptation theory [32–34] using REPTATE [29] software which is also shown along with the parameters used. The range of molecular weights, obtained using gel permeation chromatography (and shown in supplementary material B [28]), was discretised to 20 values per decade of molecular weight and used as input for the theory. Materials parameters, τ_e (Rouse time of one entanglement segment) G_e (entanglement modulus) and M_e (entanglement molecular weight) were all fitted to the data, and values are included in Fig. 3. The molecular weight of a Rouse monomer, M_0 was kept to a value of 0.001 kg/mol as recommended [35] and α, which is the dilution exponent for treating constraint release, was set to a value of 1.3, in accordance with the recommendation of Van Ruymbeke *et al*. [36]. This gave values for τ_e G_e and M_e that were consistent with established literature values for polystyrene. An estimation of the weight-averaged Rouse time can be given by

$$\tau_R = \sum^{a} \tau_e \left(\frac{M_{w_a}}{M_e}\right)^2 w_a \,, \tag{3}$$

where M_{w_a} is the molecular weight and w_a is the weight fraction of that molecular weight from the GPC. This was calculated over the range of molecular weights in the GPC, giving a value of 0.434 s. The reptation time was taken as the inverse of the low frequency crossover in G′ and G″, giving a value of 3.34 s.

It is important to note that the variety of polymer molecular weights present in even a moderately polydisperse sample implies that the material contains a mixture of chains possessing a range of Rouse (stretching) and reptation (orientation) times. In order to further explore the effect of polydispersity, the proportion of chains with Rouse and reptation Weissenberg numbers above 1 was calculated for each shear rate. The REPTATE [29] materials database was used to identify values for the molecular weights of polystyrene at 170 °C required to give a reptation Weissenberg number, Wi_d of 1 at each speed, and the GPC results were used to calculate the weight fraction of chains exceeding this molecular weight. For the Rouse times, Eq. (3) with the materials parameters from the fits was used to calculate the molecular weight corresponding to a Rouse Weissenberg Wi_R number of one. The results are summarized in Table II.

The linear rheological characterization was also repeated on a sample after the MPR experiments were performed, to check for degradation, confirming no change, which is expected for polystyrene which is relatively stable with respect to oxidation at 170 °C.

B. Multipass rheometry

In order to confirm there was no significant pressure loss over an experiment, the mean pressure (average of values at top and bottom pistons) was monitored throughout each experiment. No significant change in mean pressure was noted on starting the movement of the pistons, although the individual transducers' values changed due to the pressure drop across the geometry, as shown in Fig. 4 and observed previously for prepressurized MPR experiments by Valette *et al*. [37].

On cessation of movement, some decrease in mean pressure was noted over very long times (~10% over ~40 min

TABLE II. Calculated weight fractions of chains above their Rouse and reptation times for each piston speed used, calculated from the GPC results and using the REPTATE [24] materials database.

Speed/mm s^{-1}	Rabinowitsch corrected wall shear rate/s^{-1}	M ($Wi_d = 1$)/gmol^{-1}	Polymer chain fraction above M ($Wi_d = 1$)	M ($Wi_R = 1$) /gmol^{-1}	Polymer chain fraction above M ($Wi_R = 1$)
0.005	0.071	358 000	0.308	2 950 000	0.000891
0.01	0.14	293 000	0.381	2 080 000	0.00360
0.05	0.71	186 000	0.541	933 000	0.0503
0.1	1.4	154 000	0.607	660 000	0.118
0.5	7.1	99 600	0.730	295 000	0.379

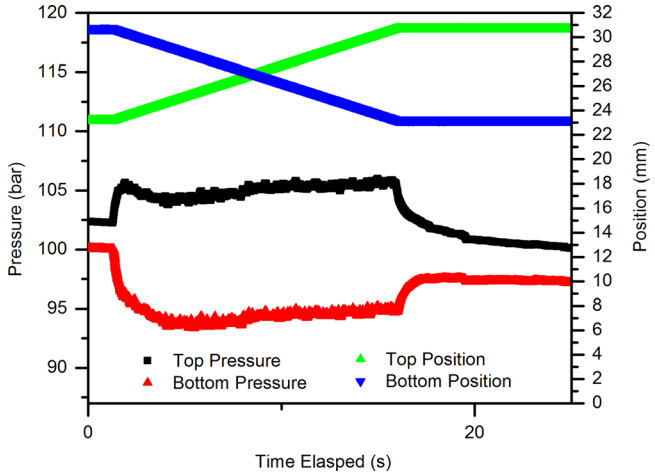

FIG. 4. Values of the pressure and position of individual transducers during an experiment at 170 °C, 100 bar initial pressure and a speed of 0.5 mm/s.

at 100 bar). However, the applied deformations were short (<1 min) and the data analysed from the stress relaxation was within the first 20 s of stopping the pistons, when the mean pressure and the recovered pressures at each piston after the decay, were not significantly different from their initial values. Hence it is valid to assume that the initial pressure applied to the sample was maintained throughout the experiment.

In each experiment, the number of observed fringes was seen to increase as the flow was established until a constant state was reached. Typical results for the build-up of fringes as flow is established are shown in Fig. 5. Once the steady state is established, it is possible to select an individual frame and measure the stress within the geometry by counting the fringes as shown in Fig. 6.

The difference between the pressure at the top and bottom transducers (the pressure drop) was calculated in order to measure the pressure drop across the geometry. The time dependence of pressure drop reveals the steady state condition, where the pistons are moving at constant velocity and the pressure drop is constant (Fig. 7). An average value of the pressure in this region was recorded.

The wall shear stress σ_w, was calculated from the steady state pressure drop, in the contraction region of the geometry according to

$$\sigma_w = \frac{Pressure\ drop\ (Pa) * Flow\ area\ (m^2)}{Wall\ surface\ area\ (m^2)}, \qquad (4)$$

where the flow area is the cross-sectional area of the contraction. The wall shear stress can be related to the number of stress fringes observed via the Stress Optic Coefficient (SOC) which was calculated. This was done for a variety of experiments at different piston speeds and pressures. An average value for the SOC of $4.9 \pm 0.2 \times 10^{-9}\,\mathrm{Pa}^{-1}$ was obtained for polystyrene, which was consistent with previously published values [38,39]. This method is discussed in more detail and the resulting plot shown in the supplementary material C [28].

C. Steady state stresses and pressure drops

The wall shear stress was obtained by two methods; first the number of fringes at the steady state was counted and multiplied by the SOC. Second, the pressure drop was measured at steady state and converted into a stress (see calculation of the SOC in supplementary material B for details [28]). The apparent shear viscosity was then calculated by dividing the steady state values of the stress by the wall shear rate. Both these methods are compared to the complex viscosity (measured in the oscillatory test) and steady shear viscosity measured using a capillary rheometer in Fig. 8. Values for the pressure dependence of viscosity, β were obtained using Eq. (1), and the results are shown in Fig. 9. β values were not extracted from the stress fringes for the two slowest speeds, because the change in the number of fringes with pressure was not above the measureable error (0.5 fringes). However, these speeds could be analyzed by the pressure drop.

D. Pressure drop decays

An example of the decay in pressure drop over the geometry, after stopping the pistons, is shown in Fig. 10. The zero

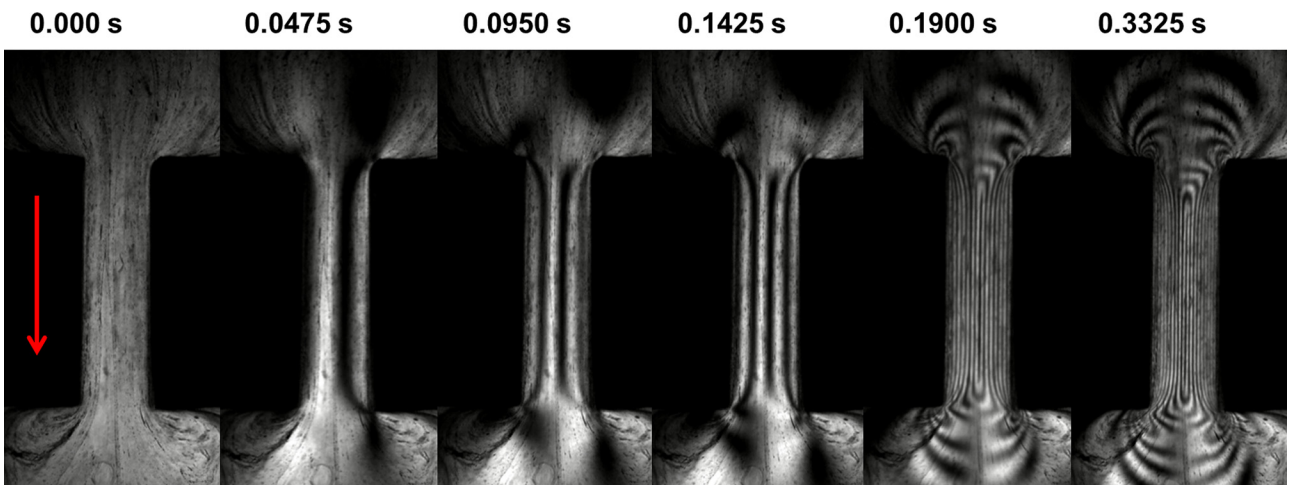

FIG. 5. Build-up of stress fringes to a steady state as PS is driven through a narrow slit at a piston speed of 0.5 mm/s under 30 bar of initial pressure at 170 °C. Arrow shows flow direction.

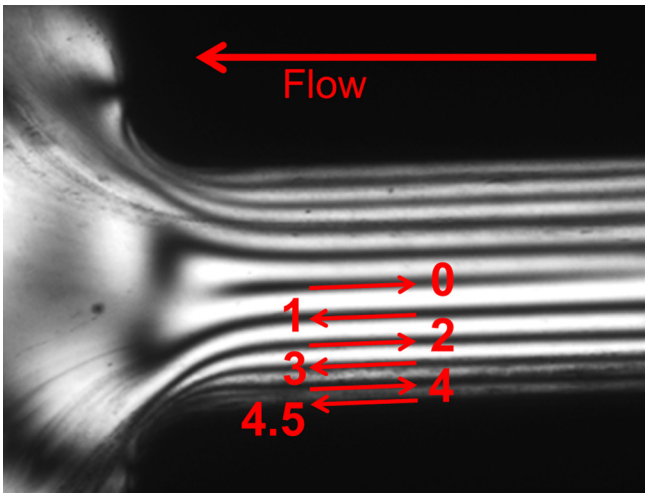

FIG. 6. Example stress birefringence image of polystyrene showing how fringes are counted outward from the zero fringe, including half a fringe counted for the dark area at the wall. Speed is 0.125 mm/s at 200 °C under 1 bar of initial pressure.

time (when the pistons stopped) was calculated from the starting time and the duration of the deformation. It was noted that the pressure drop did not return to zero over the window of observation. Because all the stress fringes had decayed at this time, it is valid to assume that this was not due to relaxation in the slit.

The pressure decays could not be represented by a single exponential decay. However, a combination of exponentials with different relaxation times gave good fits. In some decays, as many as three regions were observed, as there was seen an initial fast decay, at short times (usually < 0.1 s) in addition to two slower relaxation timescales. Hence the pressure drop decays could be fit with a three term exponential decay, including an offset term, given by

$$\frac{\Delta P}{\Delta P_0} = y_0 + A_p \exp\left(-\frac{t}{\tau_1}\right) + B_p \exp\left(-\frac{t}{\tau_2}\right) + (1 - A_p - B_p)\exp\left(-\frac{t}{\tau_f}\right), \quad (5)$$

where ΔP is the pressure drop, ΔP_0 is the initial pressure drop, t is the time after pistons are stopped, y_0 is the fitted offset, τ_1, τ_2, and τ_f are the fitted timescales and A and B are fitted magnitudes of the decays. τ_1 is an early relaxation time which appears to correspond to Rouse behavior, τ_2 is a late relaxation time which is consistent with the timescale of reptation and τ_f is included to represent the initial fast decay. The coefficients A and B therefore represent the relative contributions of the early and late relaxation processes, respectively. Although the initial fast decay may not be exponential, it is so brief that it can be approximated by including a single exponential term alongside the early and late relaxations, giving Eq. (5).

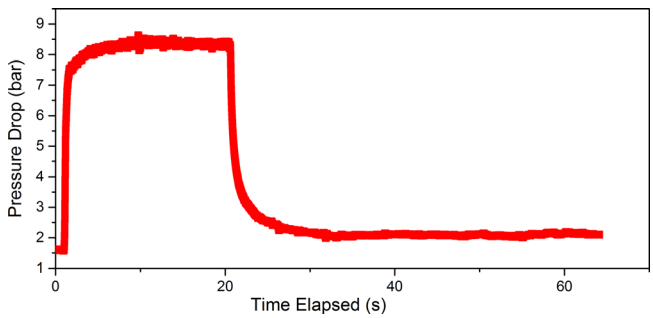

FIG. 7. Pressure drop over the contraction-expansion geometry for PS at 0.5 mm/s and 170 °C, with 30 bar of initial pressure, showing the initial build up to a steady state and then decay.

As most decays were at shear rates slower than the calculated inverse Rouse time, the τ_1 term was not always necessary. τ_1 was noted at the three highest shear rates, where the late relaxation time was observed at all shear rates. Also τ_f was only observed at the highest shear rates. For the lower shear rates, the effect of the initial fast decay was not significant enough to be observed, so the τ_f term could also be excluded. The decays were fitted using the minimum possible number of terms that yielded significantly different relaxation times. The magnitudes of the fast and early relaxation times were similar in all experiments but the fast relaxation time was always below 0.21 s and could be distinguished from the early relaxation time. All the parameters of the fits and their uncertainties are given in supplementary material C [28].

E. Stress decays

As the video recording was started independently to the piston movement, the zero point for the decays was instead taken as the point at which the fringes begin to decay. The stress analysis has been focussed on the three highest shear rates because they show sufficient fringes to allow accurate characterization of the stress decay within the error of counting the fringes. Examples of these decays can be seen in Fig. 11.

Multiple exponential decays were again necessary in order to fit the stress relaxation process; the stress decays were fitted to an exponential decay with

$$\frac{\sigma}{\sigma_0} = y_0 + A_\sigma \exp\left(-\frac{t}{\tau_1}\right) + B_\sigma \exp\left(-\frac{t}{\tau_2}\right) + (1 - A_\sigma - B_\sigma)\exp\left(-\frac{t}{\tau_f}\right), \quad (6)$$

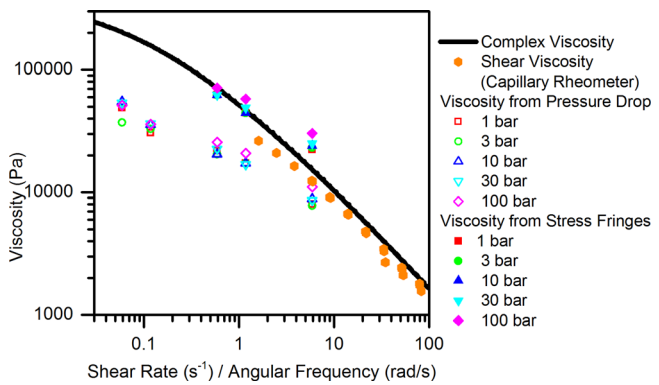

FIG. 8. Comparison of the viscosity at 170 °C measured from the fringe count and pressure drop at the steady state with the complex viscosity extracted from oscillatory rheology and steady state viscosity from capillary rheometry.

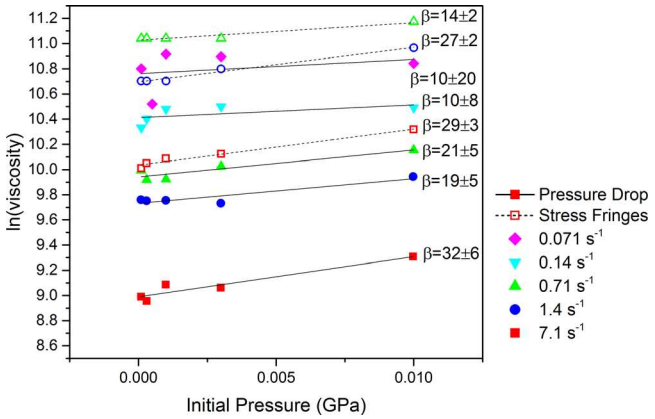

FIG. 9. Steady state viscosities at 170 °C measured from pressure drop and stress fringes, labeled with gradients in GPa^{-1}, equal to β in Eq. (1). Pressure drop data are represented by solid symbols and solid lines. Stress birefringence data are shown as open symbols and dotted lines. The two slowest shear rates did not create enough stress fringes to capture a change with pressure above the error (0.5 fringes) and hence the viscosities from stress fringes are not included.

where σ is the stress, σ_0. is the initial stress, t is the time after pistons are stopped, y_0. is the fitted offset, τ_1, τ_2 and τ_f are the fitted timescales and A and B are fitted magnitudes of the decays. Because the stress decayed to zero in every case, the offset term, was constrained to +/− half a fringe (∼5000 Pa) to account for any error in fringe counting. This approach gave good fits to the observed stress decays for all of the data (see Fig. 11). The early relaxation time, τ_1, was typically of the order of 1 s or less, and was consistently observed at the highest speed, and in some of the decays at lower speeds. The late relaxation τ_2 was observed at all speeds, and was generally found to be in the range 1–4 s. The initial fast decay τ_f was seen to be most significant at the highest speeds and pressures.

F. Relaxation times

The early and late relaxation times were found to agree well with the Rouse and reptation times, respectively, determined from the linear rheology and scaling. Both early and late relaxation times were seen to increase with applied pressure (Fig. 12). The relaxation times from both the pressure drop and stress fringes were compared and were seen to give similar values but the pressure drop results produced significantly more variation. No clear dependence of the relaxation

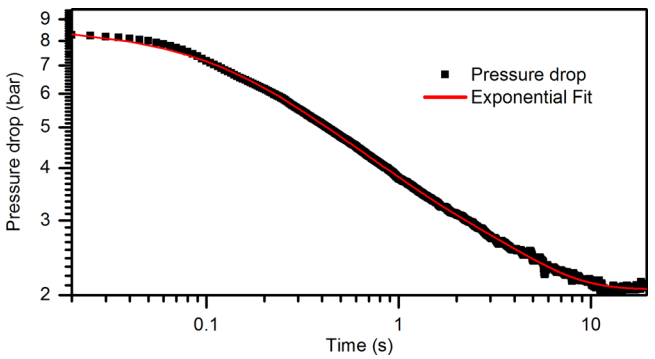

FIG. 10. Pressure drop decay of polystyrene after a deformation at 7.1 s^{-1} and 170 °C with 30 bar initial pressure applied. The curve is the result of a multiexponential fit using Eq. (4).

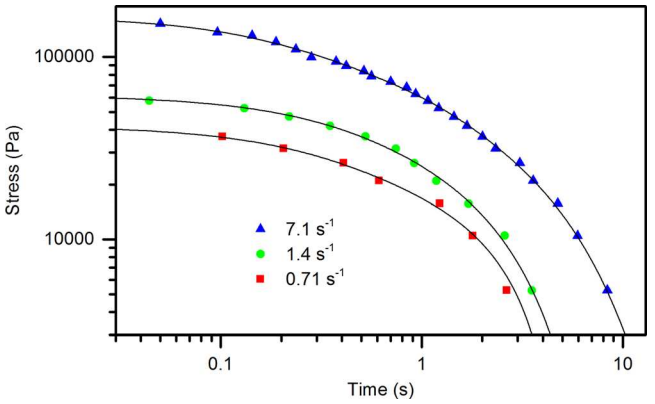

FIG. 11. Stress decays at 100 bar of initial pressure at 170 °C, shown with the exponential fits using Eq. (6) (black lines).

time with shear rate was noted (Fig. 13). Hence an average of the late relaxation time could be calculated across the different shear rates, which reduced the variation and still showed a positive relationship with pressure (Fig. 14). To quantify this relationship, they were fitted with beta values according to the equations

$$\beta_E = \frac{d\,ln(\tau_1)}{dp}, \tag{7}$$

$$\beta_L = \frac{d\,ln(\tau_2)}{dp}, \tag{8}$$

where β_E represents the pressure dependence of the early relaxation time τ_1 and β_L represents the pressure dependence of the late relaxation time τ_2. These fits are shown in Fig. 15, all values showed a positive value above the error except the pressure drop early relaxation times for which the value is of the same magnitude as the error.

IV. DISCUSSION

A. Shear rheology

The fit to the data in Fig. 3 captures the terminal crossover and rubbery region well, although slightly overestimates the

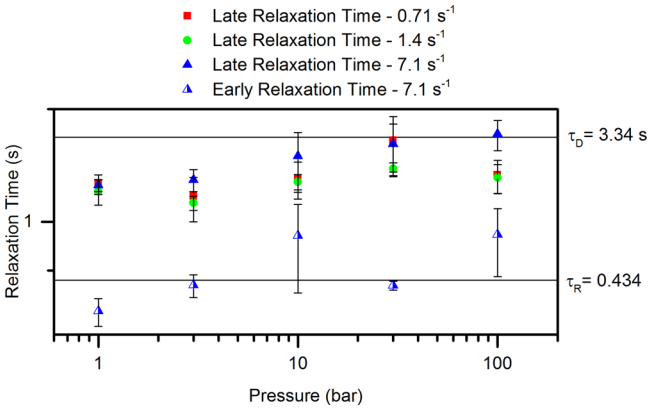

FIG. 12. Early (τ_1) and late (τ_2) relaxation times at 170 °C extracted from exponential fits of the stress decays at different pressures using Eq. (5). The Rouse and reptation times obtained from oscillatory rheology at 1 bar are annotated as horizontal lines for comparison.

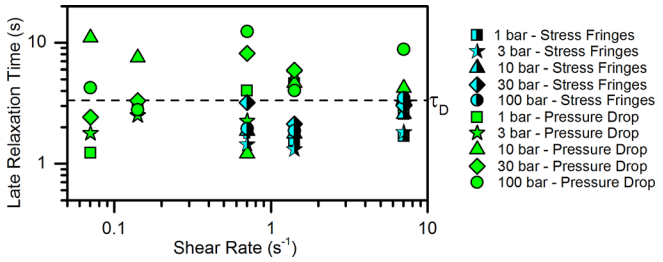

FIG. 13. Late (reptation) relaxation times at 170 °C shown at different shear rates (proportional to piston speed, see Table I). Both those obtained from exponential fits of the stress and pressure drop decays are shown, the pressure referred to is the initial pressure applied before the shear. The reptation time obtained from oscillatory rheology at 1 bar (3.34 s) is annotated as a horizontal line for comparison.

complex moduli in the terminal region. In the GPC curve (supplementary material A [28]), a small step can be seen at the lowest molecular weight, which could indicate some lower molecular weight chains were not detected. The presence of additional short chains could have contributed to the difference in the terminal region, although these also would be expected to have an effect on the plateau modulus. Nevertheless, the key features of the data for determination of characteristic relaxation times of the polymer are well captured by this model which uses the measured molecular weight distribution data as input parameters.

The reptation time from the REPTATE [29] materials database is 9.24 s for 315 k monodisperse linear PS at 170 °C. The inverse of the crossover of G′/G″ in the linear rheology differs significantly from this, giving a value of 3.34 s. The polydispersity of the sample, particularly the inclusion of shorter chains, causes this shift to a faster reptation time. The Rouse time is less dependent on the polydispersity and the value extracted from the fit to data (0.434 s) is similar to the expected value for monodisperse 315 K polystyrene (0.379 s from the REPTATE [29] materials database).

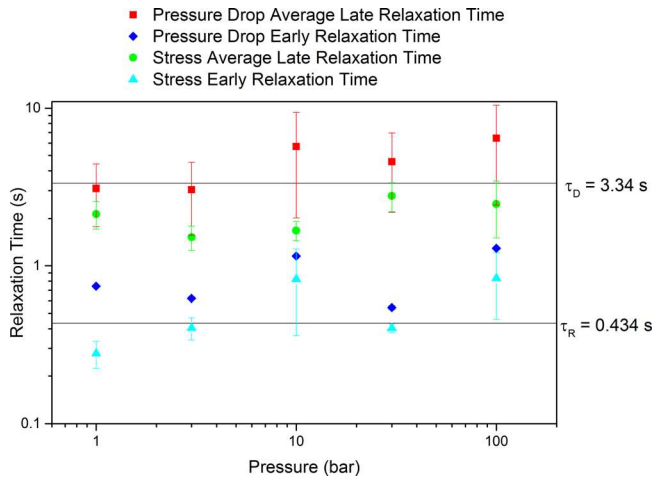

FIG. 14. Early and late relaxation times at 170 °C calculated from fits to both pressure drop and stress decays. The late relaxation times are averaged over all shear rates, whereas the early relaxation time is only seen at the highest shear rate. The Rouse and reptation times obtained from oscillatory rheology at 1 bar are annotated as horizontal lines for comparison.

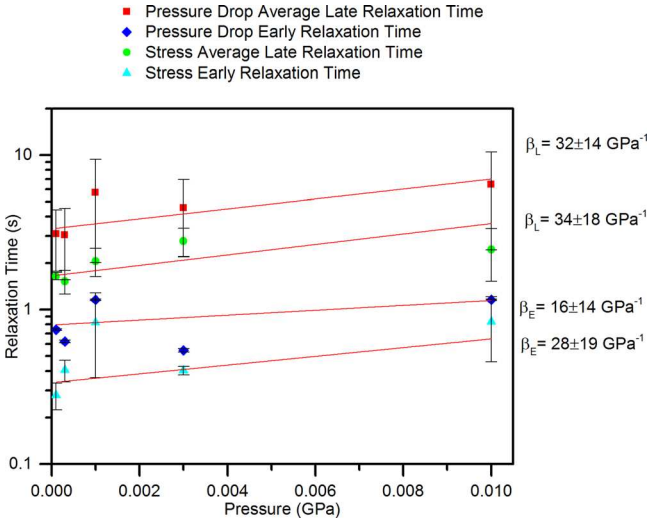

FIG. 15. Early and late relaxation times at 170 °C calculated from fits to both pressure drop and stress decays, with fits to show the trend with pressure.

B. Multipass rheometry

1. Steady state stresses and pressures

The two lowest shear rates showed relatively little build-up of stress (1–1.5 fringes). At these piston speeds, the wall shear rates are below the inverse reptation time and so the polymers can fully relax on a shorter timescale than it takes to build up a deformation of order 1. On this basis, it might be considered surprising that any stress fringes at all are observed, since Wi_R is much less than one. However, the calculated data in Table II show there is a significant proportion of chains that are above their inverse reptation times at all piston speeds, and a small fraction may even fall into the $Wi_R > 1$ regime. The faster speeds showed significantly higher stress birefringence as an increasing proportion of the molecular weight distribution is unable to relax.

The extracted viscosities and β values are included here as a method of comparing results with existing literature and ensure consistency before discussing the more novel stress decays. Steady shear data from a capillary rheometer is provided alongside the complex viscosity extracted from the oscillatory measurements, the two show good agreement and demonstrate that the Cox-Merz rule [40] holds for this material.

The viscosities extracted from the fringe counting were significantly higher than for the pressure drop results at the same speed, and the values from fringe counts showed better agreement with the complex viscosity. This is due to the contribution of the entry and exit effects to the pressure drop which are minimized when counting fringes by only examining those in the gap. These additional contributions to the strain could have reduced the viscosity of the material (since it is a shear thinning polymer). The stress calculated from the pressure drop is therefore lower than that from fringe counting, which gives rise to the lower apparent viscosity.

It has been observed that β values vary when determined from different techniques (involving different methods of calculation) [17]. Comparing the β values obtained by stress fringes to those from pressure drop analysis in our experiments,

however, there is some deviation between the two methods, but it is not systematic and differences are close to the range of error (Fig. 9). The value of the SOC used could be a contributing factor as it is an average over many experiments and is seen to vary with shear rate (see supplementary material B for details [28]). The uncertainty in the SOC of $0.2 \times 10^{-9}\,\mathrm{Pa}^{-1}$ is achieved by fitting to many measurements, whereas it is of the order $1 \times 10^{-9}\,\mathrm{Pa}^{-1}$, (+/−20%) in individual measurements. There is a much greater error in the values extracted from the pressure drop and the values fluctuate more significantly. This is likely due to effects outside the slit that cause fluctuations in viscosity, and could be reduced by recording more points at different pressures should a more accurate β be required from pressure drop alone. Since at the two lowest shear rates, a change in the number of fringes with pressure could not be separated from the error (0.5 fringes), the effect measured by the change in pressure drop may not have been due to shear in the slit, and could have been dominated by exit and entry, which could have caused the anomalous results at these shear rates.

As the experiments were designed to span a logarithmic range of pressures (in order to study the stress relaxations) there is significant error introduced by fitting the limited range of points on a linear pressure scale. Despite this, it appears that values of β obtained with the MPR are in line with those obtained by other techniques. Notably, Kamal [8] obtained a value of $20.7\,\mathrm{GPa}^{-1}$ for PS at $2500\,\mathrm{s}^{-1}$ and Sedlacek *et al.* [7] obtained a shear independent (zero-shear) value of $43.45 \pm 12.1\,\mathrm{GPa}^{-1}$. Volpe *et al.* [41] reported values in the range $5–40\,\mathrm{GPa}^{-1}$, for PS at temperatures in range 220–260 °C and showed the value decreased with shear rate. As discussed in the introduction, it can be difficult to obtain reliable values of the pressure coefficient as strictly it is defined only at a specific shear rate and temperature. For the values extracted from both the stress fringes and pressure drop, β is seen to increase with shear rate. This appears to contradict some reports in literature which show an increase [10,15], or that suggest β is independent of shear rate Goubert *et al.* [42]. The β values are plotted against shear rate in supplementary material E [28].

C. Pressure drop decays

The pressure drop decays following cessation of flow were seen to follow a complex decay. This could however be modeled using several exponential decays (as in a simple Maxwell model of viscoelasticity [27]) with different timescales expected to be present in a polymer melt. There is expected to be relaxation due to both Rouse motion and reptation, which explains the presences of two different regimes, however there was also noted a third regime, very fast decay at very short times (much shorter than the Rouse time). This was seen at all pressures, although the magnitude of the decay occurring in this region increased with pressure and shear rate, making it most noticeable at the highest shear rates and pressures. This could be due to compressibility effects, which have been shown to affect the decays greatly at short times. For example, during a deformation we see pressure build up before the contraction in the geometry (causing the pressure drop across the geometry), which would cause some compression of the polymer before the geometry. On stopping the pistons, the polymer could continue to flow to recover this change in density (as the volume between the pistons is kept constant), as well as relaxing stress *via* polymer motion.

Ranganathan *et al.* [18] observed for HDPE in an MPR, the presence of different regimes in the flow curve. As piston speed was increased, they observed a discontinuity in the pressure drop which suggested a region of unstable flow. Interestingly, the equivalent flow curves for polystyrene did not show any discontinuity, suggesting all our measurements were in the region of stable flow (Fig. 16), and that flow instability cannot account for the different relaxation rates that are apparent in the stress and pressure drop decays. Ranganathan modeled pressure drop decay in this region using an adapted version of the Molenaar-Koopmans model for pressure changes during capillary flow, and showed that compressibility played an important part in the stress decay. Valette *et al.* [37] expanded on this by using Rolie-Poly [43] (based on viscoelasticity) and Carreau-Yasuda [44] (based on compressibility) models to calculate pressure drop decays for linear low density polyethylene, and showed that the decays were more dominated by compressibility effects early on and viscoelastic effects later in the decay, and the decay could be well represented using a Rolie-Poly model incorporating compressibility. We would expect our decays to be particularly dictated by the viscoelasticity of the polymer because of the broad plateau region measured in the linear rheology (and hence broad viscoelastic relaxation spectrum of the polymer). Hatzikiriakos and Dealy [45] note that short rise times to steady state (as seen in our experiments, on the scale of a few seconds) usually produce viscoelastically driven flows, and compressibility driven flows are usually characterized by rise times of several hours.

It is therefore valid to assume that the decays seen are mostly dominated by viscoelasticity. However, since compressibility effects are seen at very short times it seems unlikely that the fast decay seen in our results is part of the polymer relaxation, and therefore can be separated out from the viscoelastic relaxation times.

It was initially postulated that the fast decay could be due to the polymer continuing to flow after the pistons have stopped. However, when the flow stop time was calculated (see supplementary material F [28]) for this instrumental geometry, it was shown to be ∼9 ms. This is a shorter time

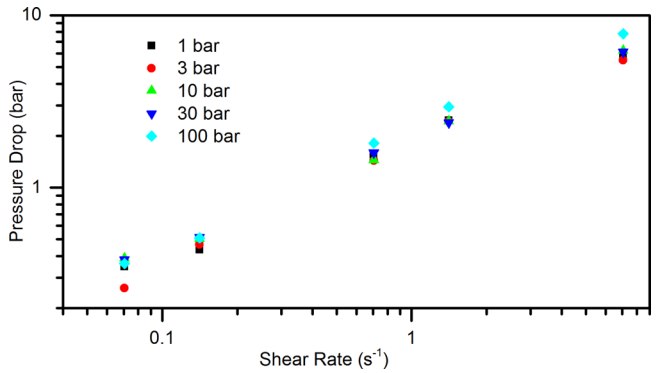

FIG. 16. Flow curve of polystyrene at all pressures at 170 °C. The points show a power law relationship and show no discontinuity.

than the frame rate of the camera, hence could not have an effect on our results. It is also unlikely that the polymer leaking into some gap or part of the system that was not fully sealed, could contribute to the fast relaxation observed. Great care was taken to fully seal the cavity, and any such loss would cause the pressure and stress to decrease during the deformation, resulting in a decrease rather than a constant steady state.

However, a very small overshoot is noted in the retreating lower piston (for example, 0.02 mm for a 15 mm stroke at 0.5 mm/s and 100 bar pressure). This overshoot is not present for the advancing top piston, and so would cause a small relaxation is pressure and stress. Despite the small magnitude of this effect with respect to the stroke amplitude, it may have caused the initial fast decay of stress observed. Careful observation of particles present in the recorded videos supports this. Observing a single particle in the flow, a stop in motion is noted on stopping the pistons, after which a little forward flow continues (Fig. 17). This suggests that there is an initial abrupt stop in movement, followed by the small overshoot in movement of the retreating piston causing the residual forwards flow (within 0.1 s of the stop in movement). This effect is likely the origin of the abnormally fast decays, which occur on a similar timescale ($\sim$0.1 s).

Predictions from linear rheology suggest the mean Rouse time should only contribute at the highest shear rate, however, it is was possible to observe the early relaxation time from experiments at 1.4 and 0.69 s^{-1}. This is consistent with our calculations from the GPC which suggest 5%–10% chains are still above their inverse Rouse times at these rates.

At shear rates exceeding the inverse reptation time, the magnitude of the pressure drop is seen to increase with shear rate, and a significant increase is seen in the number of stress fringes. Nevertheless, a significant pressure drop is observed following flow cessation after the shear rates below the inverse reptation time, as well as stress fringes (1–1.5). The GPC analysis suggests this is due to the presence of higher molecular weight chains, as at all speeds there are significant amounts of chains (>25%) above their inverse reptation time, and the longest relaxation times are predicted to dominate viscoelastic effects.

D. Stress decays

Since the pressure drop across the geometry is proportional to the wall shear stress, the stress should also be expected to decay exponentially. This is seen in our results and as with the pressure drop decays, three regimes are observed. The three term exponential fits therefore gave very good agreement with the experiment data.

As for the pressure drop, all three of these regions are only observable at the highest shear rate. The initial fast term again is most apparent at the highest shear rates and pressures. However it was not captured in many of the stress decays, likely because of the reduced frequency of points. The camera frame rate of 18 fps gives a frame every 0.0475 s and as the fast decay occurs on a timescale of around 0.1 s, there may not have been enough data to isolate it for some decays.

E. Relaxation times

The β values for calculated for the relaxation times with pressure each show a small positive value, with the exception of the pressure drop early relaxation times, which has a β value close to the level of error (as shown in Fig. 14). The pressure drop early relaxation times are expected to be the most effected by error since the pressure drop fluctuates more than the stress fringes and the early relaxation time has a lower value than the late (so is more effected by short timescale fluctuations). Both the early and late stress relaxation times show a similar increase with pressure, which implies that both the local stretching and long range orientational relaxation are retarded by increasing pressure. The increased pressure causes a slowing in molecular movement, resulting in an increase in viscosity (as seen frequently in literature, for example, [19]). This effect reduces the speed of both Rouse and reptation processes.

Overall no significant effect on relaxation time with shear rate is noted, as shown in Fig. 13. Although the shear rate can change relative contribution from each the regime of the relaxation behavior, it would not be expected to influence the Rouse or reptation relaxation times directly.

There is clearly more fluctuation in the relaxation times obtained from the pressure drop decays than the stress fringes, however, the two methods are in relatively good agreement and the early and late relaxation times are distinct from one

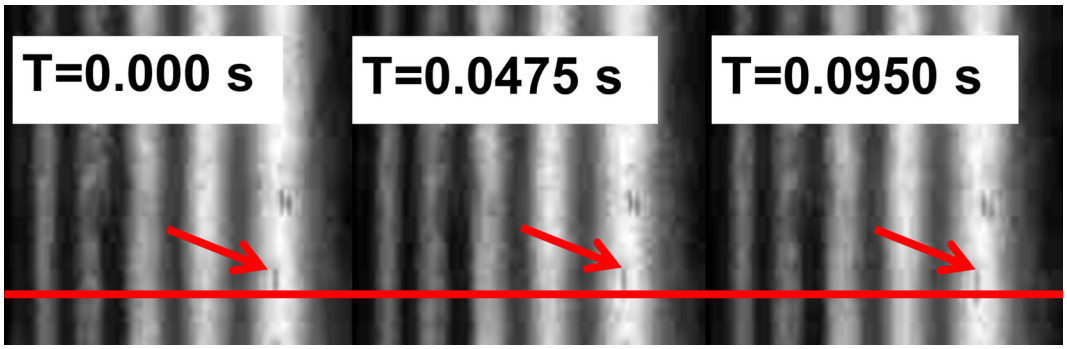

FIG. 17. First three frames of video after piston stopped (noted from fringe decay) after a deformation at 0.1 mm/s and 170 °C with 10 bar initial pressure. A particle can be seen to stop between the first two frames before continuing to move a little, indicating residual flow due to overshoot of the lower piston.

another in each case. Overall, the optical capability clearly provides a more accurate measure of the relaxation time and provides other benefits such as being able to see the distribution of stress around the geometry, allowing analysis of exit and entry effects and the identification of wall-slip effects.

It is unclear why the pressure drop gives slightly higher values for the relaxation time than the optical analysis. The offset term, necessary to facilitate the exponential fits since the pressure drop did not decay to zero, could have contributed to this difference. Despite this, the trends are consistent between methods, and using either pressure or stress data has been shown to give reliable information on the relaxation times of the polymer. This suggests relaxation times could be obtained from the pressure decays alone, e.g., for an opaque sample. Furthermore, because the nature of the MPR allows multiple experiments, multiple decays could be recorded and averaged in order to minimize fluctuations.

V. CONCLUSION

Using a multipass rheometer for the study of stress decay on cessation of a contraction-expansion flow, it has been possible to elucidate the pressure dependence of the viscoelasticity of polystyrene melts as well as several aspects of the underlying molecular rheology. Results for the pressure dependence of viscosity were broadly in line with those obtained using other methods on similar materials. The decay of stress could be described by a sum of up to three characteristic relaxation processes. The fastest process, most apparent after high shear rates and high pressures, is thought to arise from apparatus compliance in the form of an overshoot of the retreating piston. The remainder of the relaxation can be described by two characteristic time scales, which correspond well to the Rouse and reptation times of the polymer. Interestingly the stress measured is significant even at inverse shear rates slower than the mean reptation relaxation time. We believe that this is because the dispersity in molecular weight gives rise to a small fraction of material with much longer relaxation times, and significant chain orientation and even stretch are possible at low shear rates. The method is nondestructive to the sample and repeatable. With careful recording and observation of the stress fringes, relaxation times for a polymer can be extracted.

ACKNOWLEDGMENTS

The authors gratefully acknowledge financial support from Michelin R&D (Material Performance and Processability). The authors would like to acknowledge Dr. Ian Robinson (Visiting Industrial Fellow, Durham University) for initial inspiration for the work, as well as the van Reenen group (Stellenbosch University, South Africa) for use of the capillary rheometer.

References

[1] Williams, M. L., R. F. Landel, and J. D. Ferry, "The temperature dependence of relaxation mechanisms in amorphous polymers and other glass-forming liquids," J. Am. Chem. Soc. **77**, 3701–3707 (1955).

[2] Ferry, J. D., *Viscoelastic Properties of Polymers* (Wiley, New York, 1980).

[3] Dealy, J. M., and J. Wang, *Melt Rheology and Its Applications in the Plastics Industry* (Springer, Netherlands 2013).

[4] Barus, C., "Note on the dependence of viscosity on pressure and temperature," Proc. Am. Acad. Arts Sci. **27**, 13–18 (1891).

[5] Miller, A. A., "Analysis of the melt viscosity and glass transition of polystyrene," J. Polym. Sci. A-2: Polym. Phys. **6**, 1161–1175 (1968).

[6] Utracki, L. A., and T. Sedlacek, "Free volume dependence of polymer viscosity," Rheol. Acta **46**, 479–494 (2007).

[7] Sedlacek, T., M. Zatloukal, P. Filip, A. Boldizar, and P. Saha, "On the effect of pressure on the shear and elongational viscosities of polymer melts," Polym. Eng. Sci. **44**, 1328–1337 (2004).

[8] Kamal, M. R., and H. Nyun, "The effect of pressure on the shear viscosity of polymer melts," Trans. Soc. Rheol. **17**, 271–285 (1973).

[9] Volpe, V., and R. Pantani, "Effect of pressure on viscosity at high shear rates by using an injection molding machine," AIP Conf. Proc. **1695**, 020060 (2015).

[10] Sorrentino, A., and R. Pantani, "Pressure-dependent viscosity and free volume of atactic and syndiotactic polystyrene," Rheol. Acta **48**, 467–478 (2009).

[11] Sorrentino, A., and R. Pantani, "Determination of the effect of pressure on viscosity of an isotactic polypropylene," Polym. Bull. **70**, 2005–2014 (2013).

[12] Kadijk, S. E., and B. H. A. A. Van Den Brule, "On the pressure dependency of the viscosity of molten polymers," Polym. Eng. Sci. **34**, 1535–1546 (1994).

[13] Akdeniz, G., U. Yahsi, and C. Tav, "Viscous behavior of PS, PP, and ABS in terms of temperature and pressure-dependent hole fraction," J. Appl. Polym. Sci. **117**, 110–113 (2010).

[14] Fernández, M., M. E. Muñoz, and A. Santamaría, "A combined analysis of PVT and rheological measurements: Novel results for three amorphous polymers," Macromol. Chem. Phys. **209**, 1730–1737 (2008).

[15] Cardinaels, R., P. Van Puyvelde, and P. Moldenaers, "Evaluation and comparison of routes to obtain pressure coefficients from high-pressure capillary rheometry data," Rheol. Acta **46**, 495–505 (2007).

[16] Park, H. E., and J. M. Dealy, "Effects of pressure and supercritical fluids on the viscosity of polyethylene," Macromolecules **39**, 5438–5452 (2006).

[17] Park, H. E., S. T. Lim, H. M. Laun, and J. M. Dealy, "Measurement of pressure coefficient of melt viscosity: Drag flow versus capillary flow," Rheol. Acta **47**, 1023–1038 (2008).

[18] Ranganathan, M., M. Mackley, and P. Spitteler, "The application of the multipass rheometer to time-dependent capillary flow measurements of a polyethylene melt," J. Rheol. (1978-present) **43**, 443–451 (1999).

[19] Mackley, M. R., and P. H. J. Spitteler, "Experimental observations on the pressure-dependent polymer melt rheology of linear low density polyethylene, using a multi-pass rheometer," Rheol. Acta **35**, 202–209 (1996).

[20] Aho, J., and S. Syrjälä, "Measurement of the pressure dependence of viscosity of polymer melts using a back pressure-regulated capillary rheometer," J. Appl. Polym. Sci. **117**, 1076–1084 (2010).

[21] Friesenbichler, W., I. Duretek, J. Rajganesh, and S. R. Kumar, "Measuring the pressure dependent viscosity at high shear rates using a new rheological injection mould," Polimery **56**, 58–62 (2011).

[22] Housiadas, K. D., "Internal viscoelastic flows for fluids with exponential type pressure-dependent viscosity and relaxation time," J. Rheol. **59**, 769–791 (2015).

[23] Tsolou, G., V. A. Harmandaris, and V. G. Mavrantzas, "Molecular dynamics simulation of temperature and pressure effects on the

intermediate length scale dynamics and zero shear rate viscosity of cis-1, 4-polybutadiene: Rouse mode analysis and dynamic structure factor spectra," J. Non-Newtonian Fluid Mech. **152**, 184–194 (2008).

[24] Floudas, G., C. Gravalides, T. Reisinger, and G. Wegner, "Effect of pressure on the segmental and chain dynamics of polyisoprene. Molecular weight dependence," J. Chem. Phys. **111**, 9847–9852 (1999).

[25] Mackley, M., R. Marshall, and J. Smeulders, "The multipass rheometer," J. Rheol. (1978-present) **39**, 1293–1309 (1995).

[26] Mackley, M. R., and D. G. Hassell, "The multipass rheometer a review," J. Non-Newtonian Fluid Mech. **166**, 421–456 (2011).

[27] Gargallo, L., and D. Radic, *Physicochemical Behavior and Supramolecular Organization of Polymers* (Springer, Netherlands, 2009).

[28] See supplementary material at https://doi.org/10.1122/1.5012969 for the gel permeation chromatogram of the polystyrene, details of the calculation of the stress optic coefficient, the fitting parameters for the exponential fits to the stress, the dependence of the pressure coefficient on shear rate, details of the calculation of the flow stop time and calculation of the pressure dependence of the relaxation times.

[29] Ramirez, J., and A. E. Likhtman, "Rheology of entangled polymers: Toolbox for the analysis of theory and experiments," Reptate, http://www.reptate.com.

[30] Bagley, E., "End corrections in the capillary flow of polyethylene," J. Appl. Phys. **28**, 624–627 (1957).

[31] Rabinowitsch, B., "Über die viskosität und elastizität von solen," Zeitschrift Phys. Chem. **145**, 1–26 (1929).

[32] Likhtman, A. E., and T. C. B. McLeish, "Quantitative theory for linear dynamics of linear entangled polymers," Macromolecules **35**, 6332–6343 (2002).

[33] Viovy, J. L., M. Rubinstein, and R. H. Colby, "Constraint release in polymer melts: tube reorganization versus tube dilation," Macromolecules **24**, 3587–3596 (1991).

[34] Des Cloizeaux, J., "Relaxation of entangled polymers in melts," Macromolecules **23**, 3992–4006 (1990).

[35] Vorselaars, B., "Theory documentation: Polydisperse double reptation," *Rheology of Entangled Polymers: Toolbox for the Analysis of Theory and Experiments* (Reptate, http://www.reptate.com).

[36] Van Ruymbeke, E., C.-Y. Liu, and C. Bailly, "Quantitative tube model predictions for the linear viscoelasticity of linear polymers," Rheol. Rev. **2007**, 53–134 (2007).

[37] Valette, R., M. R. Mackley, and G. H. F. del Castillo, "Matching time dependent pressure driven flows with a Rolie Poly numerical simulation," J. Non-Newtonian Fluid Mech. **136**, 118–125 (2006).

[38] Venerus, D., S.-H. Zhu, and H. Öttinger, "Stress and birefringence measurements during the uniaxial elongation of polystyrene melts," J. Rheol. (1978-present) **43**, 795–813 (1999).

[39] Coventry, K., "Cross-slot rheology of polymers," Ph.D. thesis (University of Cambridge, 2006).

[40] Cox, W. P., and E. H. Merz, "Correlation of dynamic and steady flow viscosities," J. Polym. Sci. **28**, 619–622 (1958).

[41] Volpe, V., and R. Pantani, "Determination of the effect of pressure on viscosity at high shear rates by using an injection molding machine," J. Appl. Polym. Sci. 45277 (2017).

[42] Goubert, A., J. Vermant, P. Moldenaers, A. Göttfert, and B. Ernst, "Comparison of measurement techniques for evaluating the pressure dependence of the viscosity," Appl. Rheol. **11**, 26–37 (2001).

[43] Likhtman, A. E., and R. S. Graham, "Simple constitutive equation for linear polymer melts derived from molecular theory: Rolie–Poly equation," J. Non-Newtonian Fluid Mech.s **114**, 1–12 (2003).

[44] Yasuda, K., R. C. Armstrong, and R. E. Cohen, "Shear flow properties of concentrated solutions of linear and star branched polystyrenes," Rheol. Acta **20**, 163–178 (1981).

[45] Hatzikiriakos, S. G., and J. M. Dealy, "Start-up pressure transients in a capillary rheometer," Polym. Eng. Sci. **34**, 493–499 (1994).